Last Step of the Para Route of the Kolbe−Schmitt Reaction

Zoran Marković and Svetlana Marković*

Faculty of Agronomy, University of Kragujevac, 34 Cara Dušana, 32000 Čačak, Serbia, and Faculty of Science, University of Kragujevac, 12 Radoja Domanovića, 34000 Kragujevac, Serbia

Received August 9, 2007

This work is an extension of our investigations of the Kolbe−Schmitt reaction mechanism. The last step in the para route of the carboxylation reaction of alkali metal phenoxides is investigated at the B3LYP/LANL2DZ level of theory. Among several examined pathways, two mechanisms are proposed: the one involving a successive rearrangement of hydrogen and the other one based on the formation of free radicals. The former pathway is energetically comparable to the last step of the carboxylation reaction in the ortho position, whereas the latter pathway requires higher activation energy. Bearing in mind that the Kolbe−Schmitt reaction is performed at high temperatures, we assume that both reaction paths are plausible.

INTRODUCTION

The Kolbe−Schmitt reaction is an important source of numerous industrial products. Although the reaction has been known for almost 160 years,[1−3] it is a subject of novel experimental and theoretical investigations.[4−12] For the experimental aspects of the Kolbe−Schmitt reaction a reader is referred to a review,[3] the papers,[4−6] and the references given therein. Here we provide a short overview of the novel theoretical investigations on the Kolbe−Schmitt reaction mechanism.

The first in a series of papers considering the Kolbe−Schmitt reaction mechanism was a DFT study of the carboxylation reaction of sodium phenoxide.[7] The mechanism proposed in this paper was confirmed by Achenie and Stanescu, who investigated the solvent effect on the Kolbe−Schmitt reaction kinetics.[9,10] The investigations of the Kolbe−Schmitt reaction mechanism were continued with the carboxylation reactions of lithium, potassium, rubidium, and cesium phenoxides,[8,11] thus complementing the results obtained in ref 7. It was found that the reactions of all alkali metal phenoxides with carbon dioxide occurred via very similar reaction mechanisms with similar energy profiles. It was shown that the reactions could proceed in the ortho and para positions. The exception was lithium phenoxide which yielded only salicylic acid in the Kolbe−Schmitt reaction.[8,11] The reaction in both ortho and para positions proceeded via three transition states and three intermediates. The structure of the initially formed alkali metal phenoxide−carbon dioxide complex was elucidated.[12] It was shown that the yield of the para substituted product increased with increasing the ionic radius of the alkali metal used.[8] A quantitative explanation for this occurrence and the equilibrium behavior of the Kolbe−Schmitt reaction was provided.[7,8] The proposed mechanism was in good accord with the experimental findings on the Kolbe−Schmitt reaction: with the NMR and IR spectra of the alkali metal phenoxide−carbon dioxide complex, equilibrium behavior of the reaction, conditions of temperature and pressure, and ratio between the ortho and para products.[1−6]

In refs 7, 8, and 11 the last step of the Kolbe−Schmitt reaction in the para position was not studied in detail. The aim of this work is to fill this gap. Thus, we investigate the last step in the para route of the carboxylations of sodium, potassium, rubidium, and cesium phenoxides.

METHODS

To provide the compatibility of the results of this work with the findings of our previous investigations,[7,8,11,12] we use the same computational methods. Thus, geometrical parameters of all stationary points and transition states for the carboxylation reactions of sodium, potassium, rubidium, and cesium phenoxides are optimized in vacuum, at the B3LYP/LANL2DZ level of theory,[13−19] using the GAUSSIAN98 program package.[20] The vibrational analysis and the natural bond orbital (NBO) analysis[21,22] are performed for all structures. All the fully optimized transition-state structures are confirmed by the existence of a sole imaginary frequency, whereas the optimized intermediate structures possess only real frequencies. From the transition-state structures, the intrinsic reaction coordinates (IRCs) are obtained, and the free energies are maximized along these paths. The last step of the carboxylation reaction of sodium phenoxide is reinvestigated by means of the CEP-31+G(d) basis set. CEP-31+G(d) uses the Stevens/Basch/Krauss ECP split-valence basis set augmented with polarization and diffuse functions on heavy atoms. It will be shown later that both basis sets provide consistent results.

RESULTS AND DISCUSSION

Several pathways are considered for the transformation of pD-M to pE-M (Figure 1). A 1,5 hydrogen shift from C4 to O8 (Figure 1a), analogous to the 1,3 hydrogen shift in oD-M,[7,8] is not plausible, due to a long distance between H11 and O8 (about 4.84 Å in all pD-Ms). In addition, a reaction of mutual exchange of hydrogen between two pD-M intermediates is not revealed (Figure 1b). On the other hand, the vicinity of electron rich double bonds to H11 indicates that this hydrogen can rearrange from C4 to C5 (or C3) and then undergo further rearrangement. Our investigation shows

* Corresponding author e-mail: mark@kg.ac.yu.

10.1021/ci700296a CCC: $40.75
Published on Web 12/28/2007

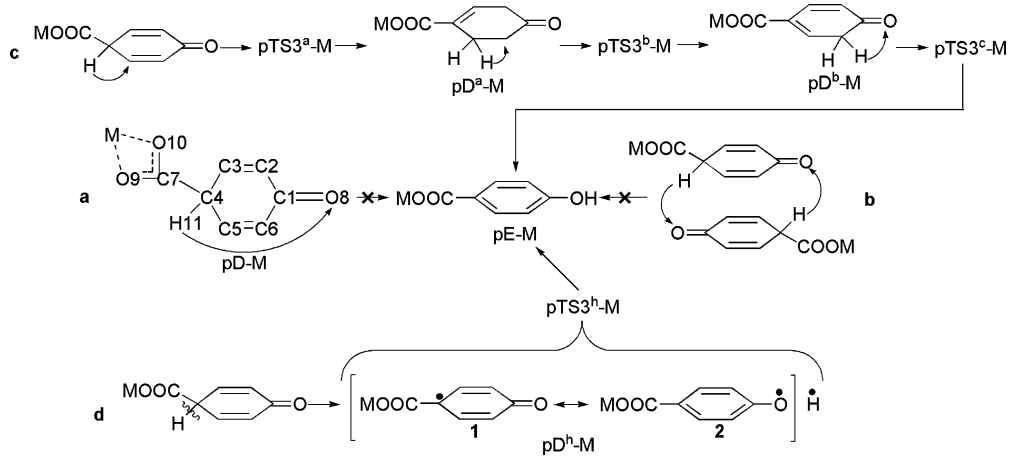

Figure 1. Examined pathways for the last step of the para route of the Kolbe−Schmitt reaction. As much as possible, we follow the notation used in ref 8. Thus, pD-M and pE-M represent the third intermediate and alkali metal salt of p-hydroxybenzoic acid. pTS3^a-M, pD^a-M, pTS3^b-M, pD^b-M, and pTS3^c-M denote further transition states and intermediates in the pathway **c**. pTS3^h-M and pD^h-M represent a transition state and free radical in the pathway **d**. M stands for any alkali metal under consideration (i.e., sodium, potassium, rubidium, and cesium), whereas chemical symbols of alkali metals are used to represent specific participants.

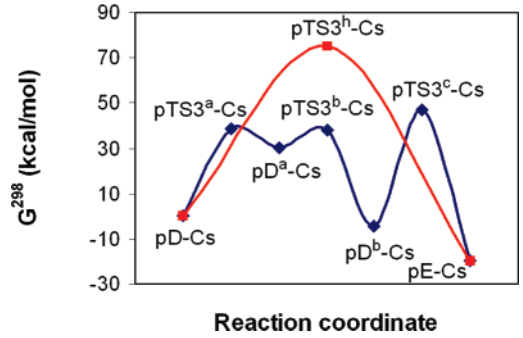

Figure 2. Two plausible paths for the conversion of pD-Cs: homolytic cleavage of the C−H bond (red line) and migration of hydrogen (blue line). Free energies are calculated relative to pD-Cs. See Figure 1 for definition of symbols.

that a migration of hydrogen from C4 to O8 occurs via three successive steps (Figure 1c), where the rate-limiting step requires an activation energy of about 51 kcal/mol. A reaction path for homolytic cleavage of the C4−H11 bond in pD-M is also revealed, with an activation energy of about 75 kcal/mol (Figure 1d).

Pathway **c** is energetically more favorable than **d** and comparable to the last step of the Kolbe−Schmitt reaction in the ortho position.[7,8,11] Taking into account that the Kolbe−Schmitt reaction is performed at high temperatures, we assume that both homolytic cleavage and migration of hydrogen are possible pathways. These two pathways will be considered in the text that follows.

The energy diagram presenting the pathways **c** and **d** is depicted in Figure 2. The values of free energies for all relevant species are given in Table 1. The values of total energies and enthalpies are very similar to the corresponding values of free energies. The free energy values for the participants in the reaction pD-Na → pE-Na, calculated with the B3LYP/CEP-31+G(d) method, are also given in Table 1. The CEP-31+G(d) basis set produces the geometries and energies very similar to those obtained by means of the LANL2DZ basis set. In other words, an introduction of polarization and diffusion functions slightly affects the outcome of the calculations. For this reason, we will further present and discuss the results of the B3LYP/LANL2DZ calculations.

Table 1. Free Energies in kcal/mol for All Relevant Species in the Last Step of the Para Route of the Carboxylation Reaction of Alkali Metal Phenoxides[a]

M	Na		K	Rb	Cs
pTS3^a-M	38.78	(36.97)	38.56	38.64	38.65
pD^a-M	29.92	(31.07)	30.22	30.43	30.29
pTS3^b-M	36.72	(35.44)	37.46	37.82	38.17
pD^b-M	−5.38	(−3.43)	−4.65	−4.29	−4.22
pTS3^c-M	45.53	(47.48)	46.61	47.09	47.61
pTS3^h-M	75.19	(77.15)	75.14	75.23	75.31
pE-M	−21.93	(−15.30)	−20.41	−19.80	−19.44

[a] The results of the B3LYP/CEP-31+G(d) calculations are given in brackets. Free energies are calculated relative to pD-M. See Figure 1 for the definition of the symbols.

A remarkable feature of Table 1 is that for any participant presented on the left, the free energy values are mutually very similar for all alkali metals. Our calculations reveal that all investigated properties show similar trends. This is in agreement with the fact that the transformations take place in the six-membered ring and are slightly dependent on alkali metals. Bearing in mind that the caboxylation reaction of cesium phenoxide yields cesium 4-hydroxybenzoate as a major product,[5] we will present the results for the transformation of pD-Cs to pE-Cs. Thus, Figure 3 presents the optimized geometries of all transition states and intermediates which appear in the reaction pD-Cs → pE-Cs.

During the course of the transformation of pD-M to pD-E, the contributions of the s and p orbitals in sp hybridization on some atoms is significantly changed. To track these changes the hybrid compositions of some bonds for all investigated intermediates where M═Cs are presented in Table 2.

MIGRATION OF HYDROGEN

The HOMOs of all pD-Ms are inspected. As an illustration the HOMO of pD-Cs is presented in Figure 4. As expected, the greatest contribution to the HOMO comes from the oxygen atoms. The HOMO also embraces the ortho (C2 and C6) and meta (C3 and C5) carbons of the six-membered ring, where the greater contribution to the HOMO comes from the ortho carbons. In addition, the natural bond orbital (NBO) charge distribution in pD-M shows that H11 is partially

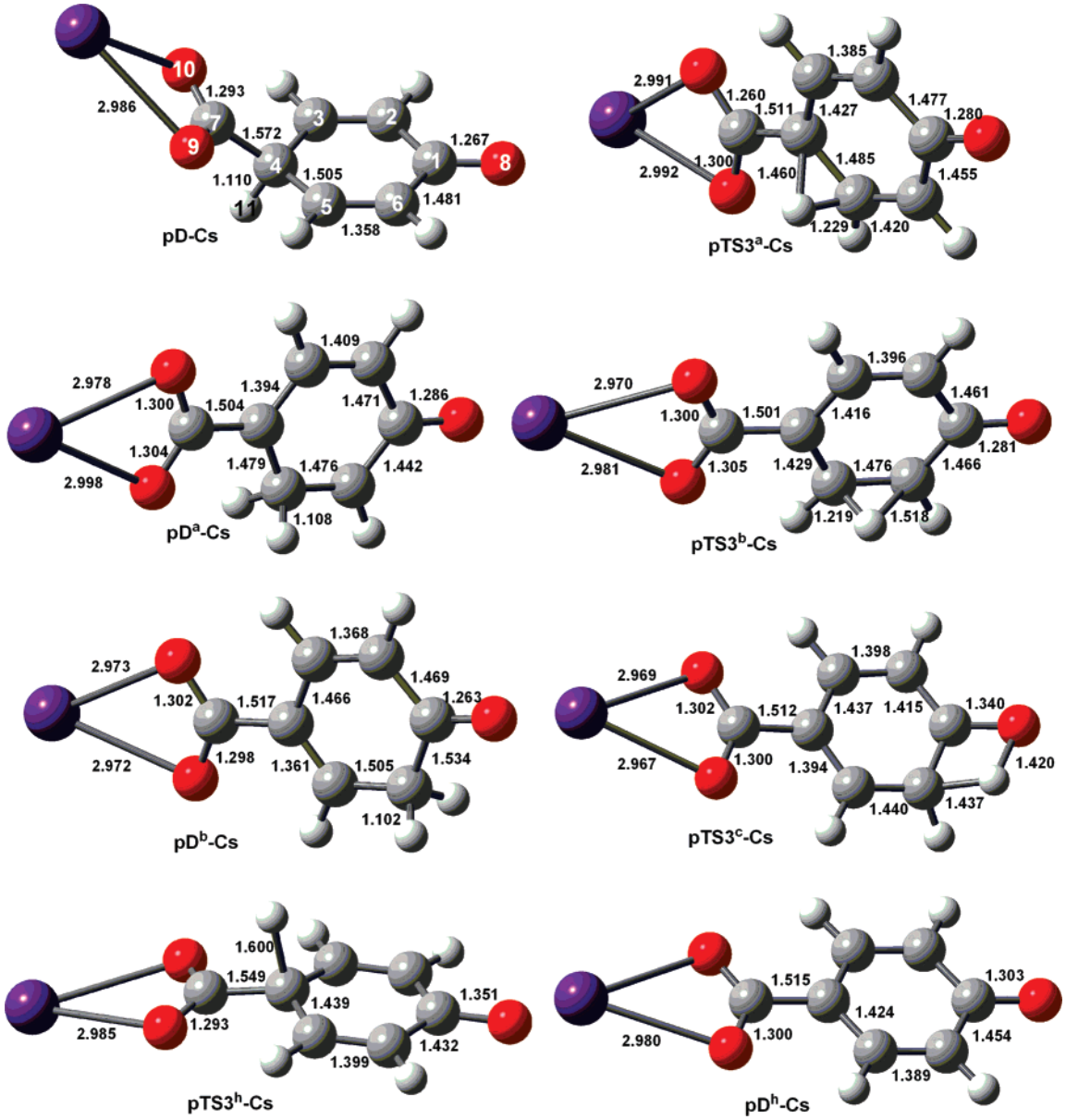

Figure 3. Optimized geometries of all relevant species in the last step of the para route of the carboxylation reaction of cesium phenoxide (see Figure 1 for definitions of symbols). Distances are given in Å. M−O bond lengths in the species containing Na, K, and Rb amount to about 2.3, 2.6, and 2.8 Å, respectively.

positively charged, whereas C5 and C6 are partially negatively charged (certainly, the charges of C3 and C2 are equal to those of C5 and C6). In pD-Cs the NBO charges of H11, C5, and C6 amount to 0.275, −0.122, and −0.299, respectively.

Both HOMO and NBO analyses indicate an rearrangement of H11 from C4 to an ortho carbon. A 1,3-shift of hydrogen is examined, but a reaction path is not found out. This is probably due to the long distance between an ortho carbon and H11 (3.150 Å in pD-Cs). Instead, the rearrangement of H11 from C4 to an ortho carbon occurs via two successive steps. These steps lead to the formation of the intermediates pD^a-M and pD^b-M via the transition states $pTS3^a$-M and $pTS3^b$-M (Figures 1 and 2). The NBO charge distribution of pD^b-M shows that H11 is partially positively charged, whereas O8 is negatively charged (0.235 and −0.608 in the case of pD^b-Cs). An attraction between these oppositely charged atoms leads to the formation of the product, via the $pTS3^c$-M transition state.

The NBO analysis of pD-M reveals three weak double bonds: C2−C3, C5−C6, and C1−O8 (Table 2), where C1−O8 is conjugated with C2−C3 and C5−C6. The hybrid composition of the C4−C7 and C4−H11 bonds shows the predominant p character with little s mixing in sp hybridization on C4. A consequence of the strong p character on C4 is that these bonds are weak. This is in agreement with the C4−C7 and C4−H11 bond lengths (Figure 3). In addition, the CO_2M group and H11 lie out of plane of the six-membered ring (by 44 and 78 ° in the case of pD-Cs).

In $pTS3^a$-M the C4−H11 bond is being broken, whereas the C5−H11 bond is being formed. The C4, C5, and H11 atoms form a three-membered ring over the six-membered ring, whereas the CO_2M group deviates from the plane of the six-membered ring only slightly (by 5° in the case of $pTS3^a$-Cs).

In pD^a-M the C4−H11 bond is completely broken. Compared to pD-M, the contribution of the s orbital in sp hybridization on C4 is increased (Table 2). As a consequence,

Table 2. Hybrid Composition of Selected Bonds for All Intermediates in the Last Step of the Para Route of the Carboxylation Reaction of Cesium Phenoxide

	hybrid composition			
bond	pD-Cs	pD^a-Cs	pD^b-Cs	pD^h-Cs
σ(C1−C6)	$0.70(sp^{1.88})_{C1}+0.71(sp^{2.09})_{C6}$	$0.70(sp^{1.91})_{C1}+0.72(sp^{1.79})_{C6}$	$0.69(sp^{1.99})_{C1}+0.72(sp^{2.63})_{C6}$	$0.70(sp^{1.83})_{C1}+0.71(sp^{1.99})_{C6}$
σ(C1−O8)	$0.58(sp^{2.27})_{C1}+0.81(sp^{1.72})_{O8}$	$0.60(sp^{2.10})_{C1}+0.80(sp^{1.91})_{O8}$	$0.58(sp^{2.25})_{C1}+0.81(sp^{1.68})_{O8}$	$0.59(sp^{2.42})_{C1}+0.81(sp^{1.96})_{O8}$
π(C1−O8)	$0.58(p)_{C1}+0.82(p)_{O8}$	$0.54(p)_{C1}+0.84(p)_{O8}$	$0.57(p)_{C1}+0.82(p)_{O8}$	$0.60(p)_{C1}+0.80(p)_{O8}$
σ(C2−C3)	$0.71(sp^{1.62})_{C2}+0.71(sp^{1.63})_{C3}$	$0.70(sp^{1.70})_{C2}+0.71(sp^{1.86})_{C3}$	$0.71(sp^{1.65})_{C2}+0.71(sp^{1.68})_{C3}$	$0.71(sp^{1.70})_{C2}+0.71(sp^{1.79})_{C3}$
π(C2−C3)	$0.73(p)_{C2}+0.68(p)_{C3}$		$0.74(p)_{C2}+0.68(p)_{C3}$	$0.71(p)_{C2}+0.71(p)_{C3}$
σ(C3−C4)	$0.70(sp^{2.06})_{C3}+0.72(sp^{2.53})_{C4}$	$0.71(sp^{1.80})_{C3}+0.71(sp^{1.81})_{C4}$	$0.71(sp^{1.97})_{C3}+0.71(sp^{2.08})_{C4}$	$0.70(sp^{1.90})_{C3}+0.71(sp^{1.89})_{C4}$
π(C3−C4)		$0.72(p)_{C3}+0.70(p)_{C4}$		
σ(C4−C5)	$0.72(sp^{2.53})_{C4}+0.70(sp^{2.06})_{C5}$	$0.70(sp^{2.09})_{C4}+0.72(sp^{2.28})_{C5}$	$0.71(sp^{1.72})_{C4}+0.70(sp^{1.64})_{C5}$	$0.70(sp^{1.90})_{C4}+0.71(sp^{1.89})_{C5}$
π(C4−C5)			$0.74(p)_{C4}+0.68(p)_{C5}$	
σ(C4−C7)	$0.74(sp^{3.13})_{C4}+0.67(sp^{1.84})_{C7}$	$0.73(sp^{2.13})_{C4}+0.68(sp^{1.76})_{C7}$	$0.73(sp^{2.25})_{C4}+0.68(sp^{1.75})_{C7}$	$0.73(sp^{2.25})_{C4}+0.68(sp^{1.76})_{C7}$
σ(C4−H11)	$0.79(sp^{4.24})_{C4}+0.61(s)_{H11}$			
σ(C5−C6)	$0.71(sp^{1.63})_{C5}+0.71(sp^{1.62})_{C6}$	$0.72(sp^{2.35})_{C5}+0.69(sp^{1.87})_{C6}$	$0.70(sp^{2.06})_{C5}+0.72(sp^{2.41})_{C6}$	$0.71(sp^{1.79})_{C5}+0.71(sp^{1.70})_{C6}$
π(C5−C6)	$0.68(p)_{C5}+0.73(p)_{C6}$			$0.71(p)_{C5}+0.71(p)_{C6}$
σ(C5−H11)		$0.80(sp^{4.03})_{C5}+0.60(s)_{H11}$		
σ(C6−H11)			$0.79(sp^{3.65})_{C6}+0.61(s)_{H11}$	

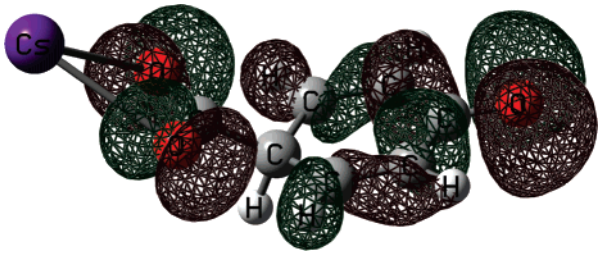

Figure 4. HOMO of pD-Cs.

the CO_2M group does not deviate from the plane of the six-membered ring. In addition, the C4−C7, C3−C4, and C4−C5 bonds are shortened (Figure 3). This particularly refers to C3−C4, which is now a double bond. This is the only double bond in the six-membered ring. A new weak C5−H11 bond is formed, with a predominant p character on C5. As a consequence, the C5−C6 bond is significantly elongated (Figure 3) and becomes a single bond. This is in agreement with the C5−C6 bond hybrid composition, which shows a decrease of the contribution of the s orbitals in sp hybridization on C5 and C6 (Table 2). The other hydrogen bonded to C5 is equivalent to H11, and they both deviate from the plane of the six-membered ring (by 54° in the case of pD^a-Cs. This provides a suitable position for one of them to perform an electrophilic attack on C6.

In pTS3^b-M the C5−H11 bond is being broken, whereas the C6−H11 bond is being formed (Figure 3). Here, the three-membered ring is composed of the C5, H11, and C6 atoms. The C4−C5 and C1−C6 bond lengths undergo significant changes.

In pD^b-M the C5−H11 bond is completely broken. In comparison to pD^a-M, the contribution of the s orbital in sp hybridization on C5 is increased (Table 2), and the C4−C5 bond is shortened (Figure 3). Now, C4−C5 becomes a double bond. The NBO analysis reveals another double bond in the six-membered ring − C2−C3. Thus, the C1−O8, C2−C3, and C4−C5 bonds form an extended π-conjugated system. A new weak C6−H11 bond is formed. Due to a decrease of the contribution of the s orbitals in sp hybridization on C6, the C5−C6 and C1−C6 bonds are elongated. Similarly as in the case of pD^a-M, two equivalent hydrogens are bonded to C6. In the case of pD^b-Cs, they lie out of the plane of the six-membered ring by 56°, at a distance from O8 of 2.700 Å.

In pTS3^c-M the C6−H11 bond is being broken, whereas the O8−H11 bond is being formed. The NBO analysis shows that C1−O8 is a single bond. The O8, C1, C6, and H11 atoms form a four-membered ring. The formation of this four-membered ring causes a deformation of the six-membered ring. Namely, the C1 atom lies out of the plane of the molecule (by 7° in the case of pTS3^c-Cs). It can be supposed that this deformation of the six-membered ring is a reason for a high activation barrier for the formation of pTS3^c-M.

Table 1 and Figure 2 show that pD^b-M is the most stable intermediate, whereas pD^a-M is far more unstable than both pD-M and pD^b-M. This can be explained with the presence of two conjugated systems in pD-M and an extended π-conjugated system in pD^b-M.

HOMOLYTIC CLEAVAGE OF THE C4−H11 BOND

So far, a possibility of formation of free radicals in the mechanism of the Kolbe−Schmitt reaction has not been considered. Taking into account the high temperatures at which the reaction is performed, it is reasonable to expect that free radicals are likely to be formed. Our calculations reveal a transformation of pD-M to pE-M via the transition-state pTS3^h-M, with an expectedly high activation energy (Table 1, Figure 2). The optimized geometry of pTS3^h-M is presented in Figure 3.

In pTS3^h-M the C4−H11 bond is being broken. As a consequence, the CO_2M group only slightly deviates from the plane of the six-membered ring (by about 9° in the case of pTS3^h-Cs). On the other hand, a deviation of C4 from the plane of the six-membered ring is observed (about 5° in pTS3^h-Cs).

Figure 2 shows that pTS3^h-M can transform to either pD-M or pE-M. In the text that follows we consider which direction for the transformation of pTS3^h-M is more favorable. For this purpose, the hydrogen atom is abstracted from pTS3^h-M, and the so-obtained free radical pD^h-M is optimized (Figure 3).

In comparison to pD-M, the NBO analysis of pD^h-M shows an increase of the contribution of the s orbitals in sp hybridization on C4 (Table 2). For this reason the pD^h-M radical becomes planar, and the C3−C4, C4−C5, and C4−C7 bonds are shortened (Figure 3). The NBO analysis reveals three double bonds in pD^h-M (Table 2). It is worth noting

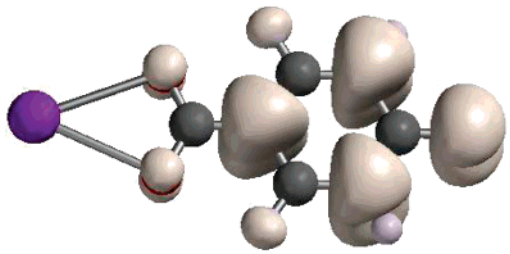

Figure 5. Spin density surface of pD^h-Cs.

that single C−C bonds are shorter than ordinary single bonds, whereas double bonds are longer than ordinary C═C and C═O bonds (Figure 3). This is in agreement with the natural resonance theory (NRT) analysis which shows that pD^h-M can be presented with two major resonance structures (pathway **d** in Figure 1). In resonance structure 1 the unpaired electron is located on C4, whereas in resonance structure 2 the unpaired electron is located on O8. The NRT resonance weightings in the equilibrium pD^h-M geometry are 30 and 47.3% for the structures 1 and 2, respectively. In addition, the spin density surface of pD^h-M (Figure 5) shows that the spin density is delocalized over the C2, C4, C6, and O8 atoms. This is in accord with the NBO analysis which shows that the natural spin density values of the C2, C4, C6, and O8 atoms amount to 0.241, 0.310, 0.241, and 0.488, whereas the values of all other atoms are very close to zero. It can be concluded, on the basis of all these facts, that the most favorable site of pD^h-M for bonding the hydrogen atom is O8. This bonding leads to the formation of pE-M.

CONCLUDING REMARKS

Two pathways are proposed for the last step of the Kolbe−Schmitt reaction of alkali metal phenoxides in the para position. The first pathway includes a rearrangement of hydrogen from C4 to O8 via three successive steps. The energy barrier for the rate-limiting step is comparable to the corresponding activation energy of the ortho route of the Kolbe−Schmitt reaction. The second step includes a homolytic cleavage of the C4−H11 bond. It is shown that highly reactive hydrogen atom bonds to O8 of the radical. The activation energy is expectedly high for radical reactions. We assume that both reaction paths are likely to occur under the experimental conditions.

This work complements the results of previous investigations of the Kolbe−Schmitt reaction mechanism.[7,8,11] With the results of this investigation the mechanism of the carboxylation reaction of alkali metal phenoxides is accomplished.

ACKNOWLEDGMENT

This work is supported by the Ministry of Science and Environment of Serbia, project no. 142025.

Supporting Information Available: Optimized geometries and total energies for all computed species: pD-M, $pTS3^a$-M, pD^a-M, $pTS3^b$-M, pD^b-M, $pTS3^c$-M, $pTS3^h$-M, pD^h-M, and pE-M. This material is available free of charge via the Internet at http://pubs.acs.org.

REFERENCES AND NOTES

(1) Kolbe, H. On the synthesis of salicylic acid. *Liebigs Ann.* **1860**, *113*, 125−127.

(2) Schmitt, R. Contribution to Kolbe's synthesis of salicylic acid. *J. Prakt. Chem.* **1885**, *31*, 397.

(3) Lindsey, A. S.; Jeskey, H. The Kolbe−Schmitt Reaction. *Chem. Rev.* **1957**, *57*, 583−620.

(4) Kunert, M.; Dinjus, E.; Nauck, M.; Sieler, J. Structure and Reactivity of Sodium Phenoxide − Following the Course of the Kolbe−Schmitt Reaction. *Chem. Ber./Recueil* **1997**, *130*, 1461−1465.

(5) Rahim, M. A.; Matsui, Y.; Kosugi, Y. Effects of Alkali and Alkaline Earth Metals on the Kolbe−Schmitt Reaction. *Bull. Chem. Soc. Jpn.* **2002**, *75*, 619−622.

(6) Kosugi, Y.; Imaoka, Y.; Gotoh, F.; Rahim, M. A.; Matsui, Y.; Sakanishi, K. Carboxylation of Alkali Metal Phenoxides with Carbon Dioxide. *Org. Biomol. Chem.* **2003**, *1*, 817−821.

(7) Marković, Z.; Engelbrecht, J. P.; Marković, S. Theoretical Study of the Kolbe−Schmitt Reaction Mechanism. *Z. Naturforsch., A: Phys. Sci.* **2002**, *57a*, 812−818.

(8) Marković, Z.; Marković, S.; Begović, N. Influence of Alkali Metal Cations upon the Kolbe−Schmitt Reaction Mechanism. *J. Chem. Inf. Model.* **2006**, *46*, 1957−1964.

(9) Stanescu, I.; Achenie, L. E. K. A Theoretical Study of Solvent Effects on Kolbe−Schmitt Reaction Kinetics. *Chem. Eng. Sci.* **2006**, *61*, 6199−6212.

(10) Stanescu, I.; Gupta, R. R.; Achenie, L. E. K. An in-silico Study of Solvent Effects on The Kolbe−Schmitt Reaction Using a DFT Method. *Mol. Simul.* **2006**, *32*, 279−290.

(11) Marković, S.; Marković, Z.; Begović, N.; Manojlović, N. Mechanism of the Kolbe−Schmitt Reaction with Lithium and Sodium Phenoxides. *Russ. J. Phys. Chem. A* **2007**, *81*, 1392−1397.

(12) Marković, Z.; Marković, S.; Manojlović, N.; Predojević-Simović, J. Mechanism of the Kolbe−Schmitt Reaction. Structure of the Intermediate Potassium Phenoxide−CO_2 Complex. *J. Chem. Inf. Model.* **2007**, *47*, 1520−1525.

(13) Becke, A. D. Density-Functional Exchange-Energy Approximation with Correct Asymptotic Behavior. *Phys. Rev. A* **1988**, *38*, 3098−3100.

(14) Lee, C.; Yang, W.; Parr, R. G. Development of the Colle-Salvetti Correlation-Energy Formula into a Functional of the Electron Density. *Phys. Rev. B* **1988**, *37*, 785−789.

(15) Becke, A. D. Density-Functional Thermochemistry. II. The Role of Exact Exchange. *J. Chem. Phys.* **1993**, *98*, 5648−5652.

(16) Hay, P. J.; Wadt, W. R. *Ab initio* Effective Core Potentials for Molecular Calculations. Potentials for the Transition Metal Atoms Sc to Hg. *J. Chem. Phys.* **1985**, *82*, 270−283.

(17) Wadt, W. R.; Hay, P. J. *Ab initio* effective core potentials for molecular calculations. Potentials for main group elements Na to Bi. *J. Chem. Phys.* **1985**, *82*, 284−298.

(18) Hay, P. J.; Wadt, W. R. *Ab initio* effective core potentials for molecular calculations. Potentials for K to Au including the outermost core orbitals. *J. Chem. Phys.* **1985**, *82*, 299−310.

(19) Dunning, T. H., Jr.; Hay, P. J. *Modern Theoretical Chemistry*; Schaefer, H. F., Ed.; Plenum: New York, 1976; Vol. 3.

(20) Frisch, M. J.; Trucks, G. W.; Schlegel, H. B.; Scuseria, G. E.; Robb, M. A.; Cheeseman, J. R.; Zakrzewski, V. G.; Montgomery, J. A., Jr.; Stratmann, R. E.; Burant, J. C.; Dapprich, S.; Millam, J. M.; Daniels, A. D.; Kudin, K. N.; Strain, M. C.; Farkas, O.; Tomasi, J.; Barone, V.; Cossi, M.; Cammi, R.; Mennucci, B.; Pomelli, C.; Adamo, C.; Clifford, S.; Ochterski, J.; Petersson, G. A.; Ayala, P. Y.; Cui, Q.; Morokuma, K.; Malick, A. D.; Rabuck, K. D.; Raghavachari, K.; Foresman, J. B.; Cioslowski, J.; Ortiz, J. V.; Baboul, A. G.; Stefanov, B. B.; Liu, G.; Liashenko, A.; Piskorz, P.; Komaromi, I.; Gomperts, R.; Martin, R. L.; Fox, D. J.; Keith, T.; Al-Laham, M. A.; Peng, C. Y.; Nanayakkara, A.; Challacombe, M.; Gill, P. M. W.; Johnson, B.; Chen, W.; Wong, M. W.; Andres, J. L.; Gonzalez, C.; Head-Gordon, M.; Replogle, E. S.; Pople. J. A. *Gaussian 98, Revision A.9*; Gaussian, Inc.: Pittsburgh, PA, 1998.

(21) Foster, J. P.; Weinhold, F. Natural hybrid orbitals. *J. Am. Chem. Soc.* **1980**, *102*, 7211−7218.

(22) Weinhold, F.; Landis, C. R. *Valency and Bonding*; Cambridge University Press: Cambridge, U.K., 2005.

CI700296A